

Banner appropriate to article type will appear here in typeset article

Linear instability in highly shear thinning fluids through a pipe

Xuerao He,¹ Kengo Deguchi,¹ Runjie Song¹ and Hugh M. Blackburn²

¹School of Mathematics, Monash University, Clayton, VIC 3800, Australia

²Department of Mechanical and Aerospace Engineering, Monash University, Clayton, VIC 3800, Australia

(Received xx; revised xx; accepted xx)

Shear-thinning fluids flowing through pipes are crucial in many practical applications, yet many unresolved problems remain regarding their turbulent transition. Using highly robust numerical tools for the Carreau-Yasuda model, we discovered that linear instability, characterised by an azimuthal wavenumber of unity, can occur. When the base flow behaves like power law fluids, two distinct unstable modes, a wall mode and a core mode, appear when the power law index falls below the critical values of 0.35 and 0.43, respectively. The viscosity ratio from infinite to zero shear rate can significantly impact instability, even if it is small, as observed in experiments. Under the parameters used in one of the experiments, where a linear critical point exists, we found that the nonlinear solutions undergo a supercritical bifurcation.

1. Introduction

Research on non-Newtonian fluids is vital for a wide range of applications, including polymer processing, food production, and biomedical engineering (Bird *et al.* 2002). The constitutive equations for these fluids are often effectively described by the power-law fluid model or its variants, such as the Carreau-Yasuda model. When the power-law index n is less than unity, the fluids exhibit shear-thinning behaviour, as observed in substances such as blood (Gijzen *et al.* (1999), Boyd *et al.* (2007)) and various industrial fluids (Carreau *et al.* (1979)). However, numerical simulations become extremely challenging as shear-thinning effect intensifies, leaving much of the flow behaviour still poorly understood.

The analysis of shear-thinning fluid flow in pipes is one of the most fundamental and practically important cases, leading to numerous experiments conducted on this subject (Escudier *et al.* (2005); Esmael & Nouar (2008); Bahrani & Nouar (2014); Charles *et al.* (2024)). Yet, even in such a simple flow configuration, many unsolved problems persist. Even on the fundamental issue of the linear stability of the laminar flow solution, experts remain divided. The purpose of this paper is to partially settle that debate.

The numerical computation community widely accepts that laminar flow is always linearly stable. This belief stems from the work of Liu & Liu (2012) and

López-Carranza *et al.* (2012), who performed a linear stability analysis using the Carreau model. Somewhat surprisingly, a systematic parameter search for the growth rates of this problem has not yet been reported, presumably because no instabilities have been observed in previous studies. Consequently, to explain the transition to turbulence, researchers have followed the analyses used for Newtonian pipe flow. For example, Liu & Liu (2012) used the idea of transient growth by Schmid & Henningson (2001), while more recent Plaut *et al.* (2017) identified finite amplitude travelling waves analogues to those found in Faisst & Eckhardt (2003); Wedin & Kerswell (2004). Pipe flow of Newtonian fluids is a classic example of shear flow that undergoes subcritical transition, with the amplitude and shape of perturbations that trigger the transition being of great interest to many researchers (Avila *et al.* 2023). Around the transitional Reynolds numbers, it is well known that the flow can be characterised by localised turbulence, called puffs (Wynanski & Champagne 1973).

Interestingly, in shear-thinning fluids, experiments have observed a transition to asymmetric mean flow profile at values below the critical threshold for puff emergence (see Charles *et al.* (2024) and references therein). While this two-step transition appears typical for strongly shear-thinning fluids, it has not yet been successfully replicated through numerical simulations to the best of the authors' knowledge. Recent experimental evidence (Picaut *et al.* 2017; Wen *et al.* 2017) suggests that the emergence of the asymmetric state might be due to the presence of supercritical bifurcations from the laminar state. Therefore, it is an intriguing question to investigate the types of linear stability that arise in non-Newtonian pipe flows and the nonlinear states that emerge from them.

In the next section, we present the mathematical formulation for shear-thinning fluid flow through a pipe, using one of the simplest types of non-Newtonian models: the generalised Newtonian model. This section also summarises the parameters, the base flow, and the numerical method used for stability analysis. §3 presents the numerically obtained neutral curves, and in §4, a bifurcation analysis is conducted. Finally, we discuss the implications of our results in §5.

2. Formulation of the problem

2.1. Governing equations

Consider an incompressible, shear-thinning fluid through an infinitely long circular pipe. We work in cylindrical coordinates (r, θ, z) , where the radial, azimuthal, and axial components of the velocity vector are denoted as u , v , and w , respectively. The velocity $\mathbf{u} = [u, v, w](r, \theta, z, t)$ and the pressure $p(r, \theta, z, t)$ are assumed to be governed by the non-dimensional incompressible Navier-Stokes equations

$$\frac{\partial \mathbf{u}}{\partial t} + \mathbf{u} \cdot \nabla \mathbf{u} = -\nabla(p + \frac{Q}{Re}z) + \frac{1}{Re} \nabla \cdot (2\mu E), \quad \nabla \cdot \mathbf{u} = 0, \quad (2.1)$$

with the strain rate tensor $E = (\nabla \mathbf{u} + (\nabla \mathbf{u})^T)/2$ and normalised dynamic viscosity $\mu(r, \theta, z, t)$. The length scale is the radius of the pipe, R^* , the velocity scale is the centre line velocity of the laminar base flow, U_c^* , and the pressure scale is $\rho^* U_c^{*2}$, where ρ^* is the density of the fluid. The scaled pressure gradient Q drives the flow. The no-slip conditions $u = v = w = 0$ are imposed on the pipe wall $r = 1$.

We adopt the Carreau-Yasuda model (Carreau 1972; Yasuda *et al.* 1981)

$$\mu = \mu_\infty + (1 - \mu_\infty) \{1 + (\lambda \dot{\gamma})^a\}^{\frac{n-1}{a}}, \quad \dot{\gamma} = \sqrt{2E : E}. \quad (2.2)$$

The Reynolds number is defined by $Re = \rho^* R^* U_c^* / \mu_0^*$, using the dimensional viscosity at zero shear rate, μ_0^* . In the model (2.2), $\mu_\infty = \mu_\infty^* / \mu_0^*$ is the viscosity ratio at infinite to zero shear rate, typically ranges from 10^{-3} to 10^{-4} , for shear-thinning fluids in experiments (Escudier *et al.* 2005, 2009). The dimensionless time constant of the fluid $\lambda = \frac{U_c^*}{R^*} \lambda^*$ can be found from the dimensional time constant, λ^* . When the Yasuda parameter a equals 2, the constitutive relation reduces to that in the Carreau model, and our non-dimensional formulation coincides with that used in Liu & Liu (2012).

2.2. Base flow

The scaled axial pressure gradient Q is determined such that the laminar base flow has a centre line velocity of unity. Substituting $(u, v, w, p) = (0, 0, \bar{w}(r), \bar{p}(r))$ into the governing equations, we find that \bar{w} and Q can be determined by solving

$$r^{-1}(r\bar{\mu}\bar{w}')' = -Q, \quad \bar{\mu} = \mu_\infty + (1 - \mu_\infty)\{1 + (\lambda|\bar{w}'|)^a\}^{\frac{n-1}{a}}, \quad (2.3)$$

subject to the boundary conditions $\bar{w}(1) = 0$, $\bar{w}(0) = 1$. Therefore, the constant Q depends on the quadruplet $(\mu_\infty, a, n, \lambda)$, but not on Re . Inviscid instability is unlikely to arise for physically relevant parameters, since the sufficient condition for stability established by Batchelor & Gill (1962) is fulfilled.

It is often common to set $\mu_\infty = 0$ for simplicity in numerical computations (e.g. Liu & Liu (2012); Plaut *et al.* (2017)), and we will also examine this idealised case in section 3.1. When λ is large, $\bar{\mu}$ can be approximated by the power-law $(\lambda|\bar{w}'|)^{\frac{n-1}{a}}$, except for a small region around the centreline of the pipe where \bar{w}' is $O(\lambda^{-1})$. The solution of (2.3) satisfying the no-slip boundary condition can be readily found as $\bar{w} = \frac{n}{n+1}(\frac{Q}{2\lambda^{n-1}})^{1/n}[1 - r^{1+1/n}] + \dots$, where the coefficient in front of the square bracket must be unity due to our choice of velocity scale. The aforementioned centreline region exists where $r = O(\lambda^{-n})$, within which the expansion $\bar{w} = 1 + \lambda^{-n-1}\bar{w}_1(\lambda^n r) + \dots$ holds with \bar{w}_1 being some function.

2.3. Parameters used in experiments

The five flow parameters $(\mu_\infty, a, n, \lambda)$ and Re defined above are useful for theoretical analysis but are not optimal for organising experimental data. We first note that to use the Carreau-Yasuda law, the constants μ_0^* , μ_∞^* , λ^* , n and a need to be found by fitting experimental data for the specific fluid in question. Since λ^* is a constant particular to the fluid, when the Reynolds number varies in the experiments, λ is not a constant but rather a quantity proportional to Re . Therefore it is more convenient to specify $\Lambda = \frac{\lambda}{Re} = \frac{\lambda^* \mu_0^*}{\rho^* R^{*2}}$ instead of λ . Note that Λ depends on the pipe radius R^* .

Another important consideration is the definition of the Reynolds number. In experiments, it is more convenient to fix the flow rate rather than the pressure gradient, and thus the bulk velocity U_b^* is used as the velocity scale. For example, Escudier *et al.* (2005) and Wen *et al.* (2017) employed the Reynolds number

$$Re_b = \frac{\rho^*(2R^*)U_b^*}{\langle \mu_{\text{wall}}^* \rangle} = \frac{4Re}{\langle \mu \rangle|_{r=1}} \int_0^1 \langle w \rangle r dr \quad (2.4)$$

using the dimensional viscosity at the wall, μ_{wall}^* . Angle brackets denote the average over θ , z , and t . For the base flow, the ratio $\frac{Re_b}{Re}$ can be computed easily.

From the argument in §2.2, when $\mu_\infty = 0$ and λ is large, $\bar{\mu}$ is $O(\lambda^{n-1})$ except

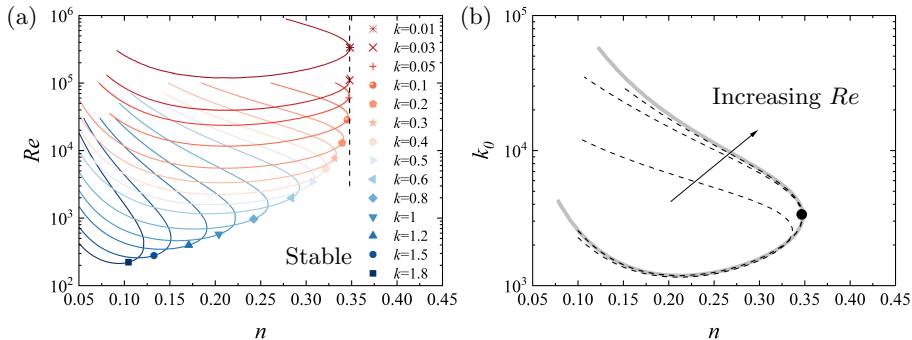


Figure 1: Linear stability for $\mu_\infty = 0$, $a = 2$. (a) Neutral curves in the $Re-n$ plane for $\lambda = 100$. The dashed line indicates the cutoff value of n for the unstable region. (b) Neutral curves in the k_0-n plane at $\lambda = 100$, where $k_0 = kRe$. The thin black dashed curves are the results for $Re = 10^4, 5 \times 10^4$, and 10^5 . The thick grey solid curve is the long-wavelength asymptotic result. The circle indicates the point used in figure 2a.

for the centre line region. Thus, in view of the viscous term in (2.1), the linear critical Re is expected to scale as $O(\lambda^{n-1})$. However, from (2.4), Re_b remains $O(\lambda^0)$, which is another reason why Re_b was favored in some previous studies.

2.4. Linear stability analysis

Our numerical code is based on the method described in Deguchi & Nagata (2011), where the poloidal-toroidal potential approach is employed. Spatial discretisation is performed using Fourier-Galerkin and Chebyshev-collocation methods. The radial basis functions follow those used in Deguchi & Walton (2013).

In the linear stability analysis, we assume the perturbation $[\tilde{u}, \tilde{v}, \tilde{w}, \tilde{p}] = [u, v, w - \bar{w}, p - \bar{p}]$ is proportional to $\exp(im\theta + ikz + \sigma t)$, where m is the azimuthal wavenumber, k is the axial wavenumber, and $\sigma = \sigma_r + i\sigma_i$ is the complex growth rate. The linear stability problem is identical to those described in Liu & Liu (2012), with a correction to the obvious typo in their equation (23). Most of our numerical results can be reproduced by LAPACK eigenvalue solvers or Rayleigh quotient iteration scheme, with 200 Chebyshev polynomials. For most parameters in this paper, the code yields very good convergence without any spurious eigenvalues. However, when the value of the λ gets large, the results need to be verified using up to 1400 Chebyshev polynomials. All the stability results presented in this paper can be reproduced using $m = 1$, as calculations for other values of m indicated smaller growth rates.

3. Linear stability results

3.1. Carreau fluids with $\mu_\infty = 0$

To obtain a general understanding of the stability characteristics of power-law like fluids, we first focus on the case where $a = 2$ and $\mu_\infty = 0$. We discovered that instability exists when n is sufficiently small. Figure 1a shows the neutral stability curves for $\lambda = 100$ for various values of k . The envelope of the curves shown in the figure gives the stability boundary in the $n-Re$ plane for $\lambda = 100$. This boundary seems to exhibit a well-defined cutoff value of n at large

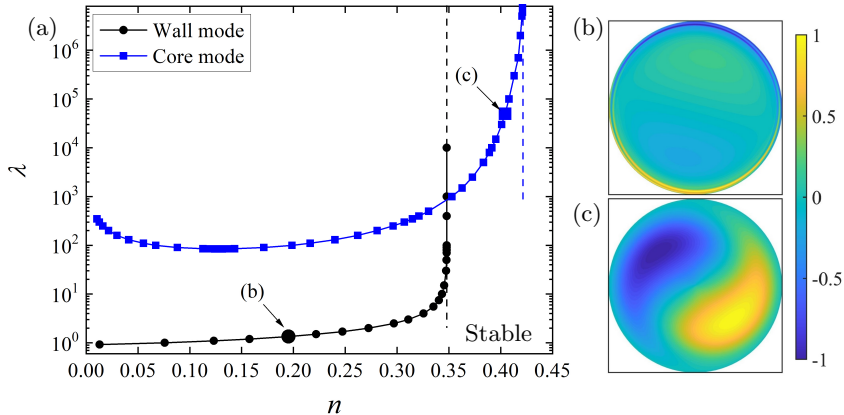


Figure 2: The long-wavelength asymptotic analysis results for $\mu_\infty = 0$, $a = 2$. (a) Neutral curves in the n - λ plane. (b) The streamwise velocity of the neutral eigenfunction for the wall mode at a pipe cross-section. The parameters used are $(\lambda, n, k_0) = (1.35, 0.195, 1.09 \times 10^5)$, corresponding to the point indicated by the arrow in panel (a). (c) The same plot as (b), but for the neutral core mode at $(\lambda, n, k_0) = (5 \times 10^4, 0.404, 0.245)$.

Reynolds numbers. As approaching the cutoff, the optimum values of k that define the stability boundary decrease. This behaviour is typical when a long-wavelength cutoff in instability occurs, as investigated by Cowley & Smith (1985) in the context of plane Couette-Poiseuille flow. In this asymptotic regime, the wavenumber is inversely proportional to the Reynolds number.

The three dashed curves in figure 1b are the neutral curves for fixed Re . Here, the vertical axis is the rescaled wavenumber $k_0 = kRe$. As Re increases, the neutral curves asymptote to the thick grey curve, which is computed using the asymptotically reduced equations. The derivation of the reduced problem, hereafter referred to as the long-wavelength limit problem, is straightforward, as it can be obtained by substituting the regular expansion $[\tilde{u}, \tilde{v}, \tilde{w}, \tilde{p}] = [Re^{-1}\tilde{u}_0, Re^{-1}\tilde{v}_0, \tilde{w}_0, Re^{-2}\tilde{p}_0] + \dots$ into the linearised Navier-Stokes equations, rescaling time as $T = Re^{-1}t$, and taking the leading-order terms.

In figure 1b, the black circle indicates the threshold value of n where instability occurs for $\lambda = 100$. Similar thresholds can be calculated for each λ , as indicated by the black circles in figure 2a. When λ exceeds about 10^3 , a new mode emerges, represented by the blue squares. We refer to these instabilities as the wall and core modes, respectively, for reasons that are evident from the flow fields shown in figures 2 (b) and (c). The wall mode is characterised by strong near the wall boundary layer structures, a large critical value of k_0 , and a small phase speed (0.123 for the case shown in figure 2b). In contrast, the core mode lacks a near wall structure, has a small critical value of k_0 , and exhibits a moderate phase speed (0.543 for the case shown in figure 2c).

As previously noted, when λ is large, the fluid viscosity exhibits power-law behaviour. Consequently, at high values of λ , the two curves in figure 2a converge toward specific values of n . While the results in the figure are derived from the long-wavelength limit, even for finite k values the wall mode is absent for $n < 0.35$, and the core mode for $n < 0.43$.

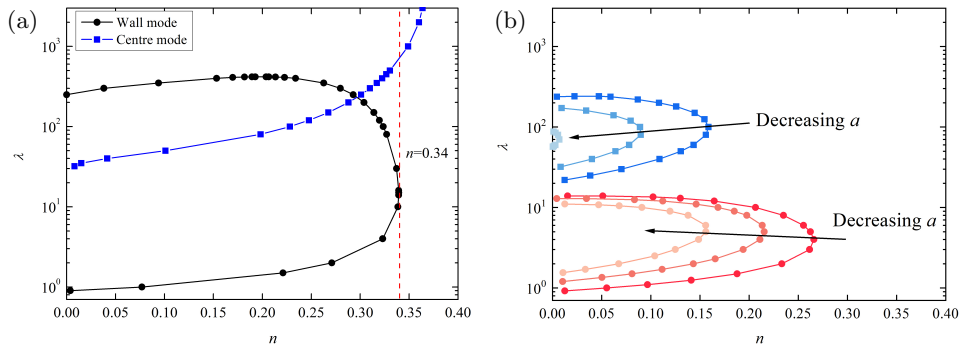


Figure 3: Similar plots to figure 2a, using different parameters (μ_∞, a) . (a) The curves with symbols are computed with $(\mu_\infty, a) = (1.207 \times 10^{-3}, 2.01)$. For comparison, the thick curves with light colour represent the results with $(0, 2)$ (same as figure 2a). The red dash-dot line indicates the value of n for 0.2% PAA as listed in Escudier *et al.* (2005). (b) The solid curves with symbols are computed using $(\mu_\infty, a) = (2.1875 \times 10^{-2}, 2.01)$. For the two families of dashed curves with a lighter color, a is set to 1.3 and 1.0, respectively. The red dash-dot line indicates the value of n for blood as provided in Boyd *et al.* (2007).

3.2. Effects of finite μ_∞

Here, we demonstrate that even small values of μ_∞ , relevant in practical applications, can significantly influence the flow dynamics. Figure 3a presents stability results derived from a long-wavelength asymptotic analysis, analogues to those in figure 2a but for $(\mu_\infty, a) = (1.207 \times 10^{-3}, 2.01)$. These values are taken from the fitting parameters for aqueous solutions of 0.2% polyacrylamide (PAA) listed in table 1 of Escudier *et al.* (2005). The fluid has an index of $n = 0.34$, indicating that the core mode may be observable, while the wall mode is likely absent.

By increasing the parameter μ_∞ to 2.1875×10^{-2} from figure 3a, the neutral curves are obtained as the solid curves in panel (b). It is evident that, as μ_∞ increases—even while remaining significantly less than unity—stabilisation occurs in the large λ parameter region. Repeating the discussion in §2.2 while keeping μ_∞ clarifies that $\mu_\infty = O(\lambda^{n-1})$ is large enough to influence the behaviour of viscosity (2.3). In fact, for $\mu_\infty \gg O(\lambda^{n-1})$, the viscosity behaves nearly Newtonian, leading to the absence of instability.

The dashed curves in figure 3b illustrate that a decrease in the value of a also contributes to stabilisation. While the two modes exist at $a = 1$, they disappear when a is reduced to 0.64. This value, along with $\mu_\infty = 2.1875 \times 10^{-2}$ and $n = 0.2128$, corresponds to the Carreau-Yasuda parameters for blood as reported in Boyd *et al.* (2007).

While figure 3 is useful for assessing whether instability occurs, identifying the physically relevant critical Reynolds number requires solving the full stability problem. Figure 4a presents the numerical results related to the experiment by Escudier *et al.* (2005). Here, following the remark in §2.3, we fix Λ and vary Re_b . The value of $\Lambda = 13.05$ is computed by $\mu_0^* = 2.94[\text{Pa s}]$, $\lambda^* = 11.1[\text{s}]$, $\rho^* = 10^3[\text{kg/m}^3]$, and $R^* = 0.05[\text{m}]$, which corresponds to the inner pipe radius of the experimental apparatus. The figure indicates that, in this case, the instability indeed appears at $Re_b = Re_{b,c} \approx 9351.9$ with the critical wavenumber $k \approx 0.0403$.

Figure 4b presents similar results using the blood parameters from Boyd *et al.*

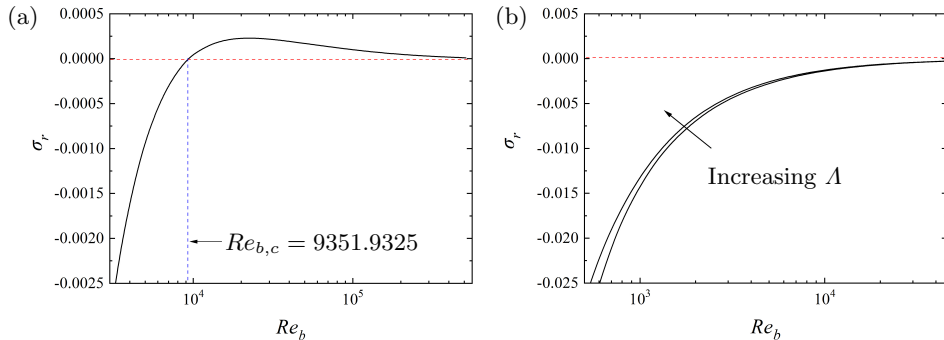


Figure 4: Growth rates σ_r of the most unstable modes, computed by the linearised Navier-Stokes equations. The value of k is optimised to achieve the maximum growth rate at each Re_b . (a) The case for 0.2% PAA in [Escudier et al. \(2005\)](#); $\mu_\infty = 1.207 \times 10^{-3}$, $a = 2.01$, $n = 0.34$, $\Lambda = 13.05$. (b) The case for blood in [Boyd et al. \(2007\)](#); $\mu_\infty = 2.1875 \times 10^{-2}$, $a = 0.64$, $n = 0.2128$. The two curves use $\Lambda = 8.13$ and 345.04 , respectively.

(2007). The two curves correspond to $\Lambda = 8.13$ and 345.04 , which are calculated based on the radii of the aorta ($2R^* = 2.54 \times 10^{-2}$ [m]) and brachial artery ($2R^* = 3.90 \times 10^{-3}$ [m]), respectively, as listed in table I of [Boyd et al. \(2007\)](#). At the highest Re_b value in the figure, λ is larger than 10^3 , which is well above the $\lambda = \mu_\infty^{1/(n-1)}$ curve in figure 3b. Thus, instability is unlikely to arise for all Re_b , aligning with the long-wavelength limit analysis. Similarly, it can be inferred that the instability observed in figure 4a should eventually stabilise as Re_b increases, though the curve $\lambda = \mu_\infty^{1/(n-1)}$ is not appearing in the range shown in figure 3a.

4. Bifurcation analysis

Bifurcation theory suggests that finite-amplitude travelling wave solutions emerge from the linear critical point identified in figure 4a. The amplitude equations, valid near the critical point, suggest that two types of solutions are possible. This is indeed true, as shown in figure 5a.

The computation of nonlinear travelling waves here utilises Newton's method implemented in the code by [Deguchi & Nagata \(2011\)](#). This code uses an analytically derived Jacobian matrix. The advantage of this method is that it avoids time integration, thereby preventing numerical instability that typically occurs when n is small. However, deriving the analytic Jacobian matrix becomes a cumbersome task as μ depends on the perturbation. This motivates us to expand μ under the small amplitude assumption, retaining only terms essential for calculating the Landau coefficient. With this weakly nonlinear approximation, the wave amplitude can be accurately determined near the bifurcation point.

We start the computation by using the neutral eigenfunction as an initial guess in Newton's method. With an appropriate choice of amplitude, the Newton iterations converge, resulting in the filled circles in figure 5a. In this bifurcation diagram, we measured the solutions by the root mean square of the fluctuation axial velocity $w' = w - \langle w \rangle$,

$$\delta = (2Re/Re_b \langle \mu \rangle|_{r=1}) \sqrt{\langle \{w'(0.8, \theta, z, t)\}^2 \rangle}, \quad (4.1)$$

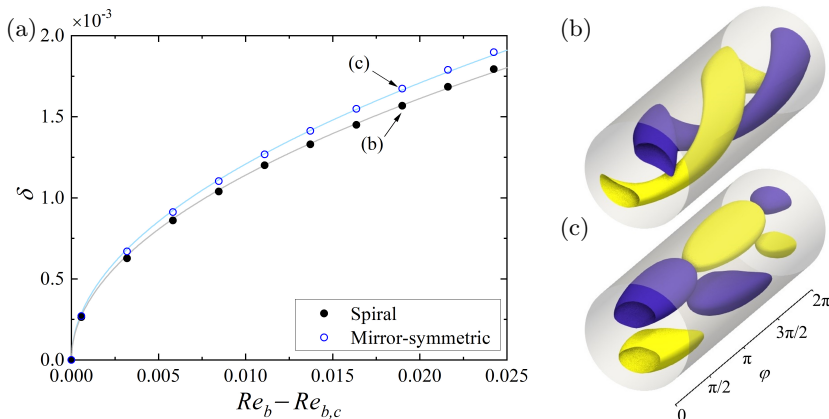


Figure 5: Bifurcation analysis from the neutral point in figure 4a. The axial wavenumber is fixed at $k = 0.0403$. (a) The bifurcation diagram near the critical point in figure 4a. Symbols are the computational results and curves are their square-root fittings. (b) The yellow/blue surface depicts the positive/negative isosurfaces of w'/δ at a magnitude of 1.5. The phase is defined by $\varphi = k(z - ct)$, where c is the phase speed of the travelling wave.

which corresponds to the quantity ‘ u'/U_B ’ in Escudier *et al.* (2005). The structure observed in the isosurface of w'/δ shown in figure 5b displays characteristics that prompt us to refer to this solution as the ‘spiral solution’. The helical invariance of the solution clearly arises from the linear neutral eigenfunction with $m = 1$.

The symmetry of the system indicates that when a helical neutral mode with a specific pitch exists, there is always another helical mode with the opposite pitch. Using a superposition of the symmetric pair of neutral modes as the initial condition for Newton’s method leads to convergence to a ‘mirror-symmetric solution’, represented by the open circles in figure 5a. The symmetry of the solution is evident from the isosurfaces shown in figure 5c.

For both solution types, the bifurcation is supercritical. The curves in figure 5a represent a square-root fit, which closely matches the symbols, indicating that the solutions computed indeed lie within the weakly nonlinear regime.

5. Conclusions and discussion

We found that the laminar state of a power-law like fluid flowing through a pipe can become unstable, exhibiting two non-axisymmetric modes (the wall and core modes), provided that both n and μ_∞ are sufficiently small. One of our key findings is that n must be below 0.43 for instability to occur. Using Carreau-Yasuda parameters corresponding to figure 7 of Escudier *et al.* (2005), which involves 0.2% PAA, we obtained a critical Reynolds number $Re_{b,c} \approx 9351.9$. From this critical point, nonlinear travelling waves (the spiral and mirror-symmetric solutions) bifurcate supercritically. This represents the first result regarding nonlinear travelling wave solutions for $n < 0.5$.

Escudier *et al.* (2005) reported that the mean flow is symmetric at $Re_b = 7695$ and 18820, but becomes asymmetric at the intermediate value of 10950. The latter value is close to the critical value we obtained, suggesting that our results seemingly support the claim of supercritical bifurcation of asymmetric states

made by [Picaud *et al.* \(2017\)](#) and [Wen *et al.* \(2017\)](#). Nevertheless, there are several important caveats to keep in mind when linking our results to experiments.

Firstly, the mean flow of our solutions do not exhibit the $m = 1$ asymmetry observed in experiments. The mean flow of the spiral solution is axisymmetric ($m = 0$), while the mirror-symmetric solution has a twofold rotational symmetry ($m = 2$). There is a possibility that the mirror-symmetric solution undergoes a symmetry-breaking bifurcation, producing the desired mean flow. However, analysing such a bifurcation would require computing the solution without the weakly nonlinear approximation used here, placing this investigation beyond the scope of the present paper.

Secondly, since the Carreau-Yasuda parameters are derived from experimental data fits, they can vary between studies even for the same surfactant concentration. This variation results from differences in the shear rate ranges used for data collection and other experimental conditions. Therefore, assuming that linear instability does not occur in experiments simply because the estimated n is greater than the theoretical cut-off value is somewhat risky.

Finally, it is important to note that most real-world non-Newtonian fluids exhibit viscoelasticity and behave in more complex fashion than for the generalised Newtonian model we used. When viscoelasticity is sufficiently strong, it is known from analyses of Oldroyd-B fluids that pipe flow can become unstable ([Garg *et al.* \(2018\)](#); [Chaudhary *et al.* \(2021\)](#); [Dong & Zhang \(2022\)](#)). Therefore, the novelty of our study lies in demonstrating that instability may arise even with small viscoelasticity. The unstable mode identified by [Garg *et al.* \(2018\)](#) is an axisymmetric ‘center mode’ (the perturbation is concentrated at the pipe centerline), which is completely different from the modes we have discovered.

Based on the values of n and μ_∞ , the case of 0.2% PAA in table 1 of [Escudier *et al.* \(2005\)](#) is identified as the most prone to instability. We also analysed other fluids in that table and found that the experiments consistently revealed an asymmetric mean flow in the cases where we detected instability. However, the reverse does not hold: asymmetry was observed even in cases without linear instability. Relating our results to asymmetric states is therefore consistent so far if viscoelasticity contributes to flow instability. To completely settle this discussion through comparisons of experiments and numerical simulations, reliable fully nonlinear solvers that incorporate shear-thinning and viscoelastic effects are essential.

Acknowledgements. This research was supported by the Australian Research Council Discovery Projects DP220103439 and DP230102188.

Declaration of Interests. The authors report no conflict of interest.

REFERENCES

- AVILA, M., BARKLEY, D. & HOF, B. 2023 Transition to turbulence in pipe flow. *Annu. Rev. Fluid Mech.* **55** (1), 575–602.
- BAHRANI, S. A. & NOUAR, C. 2014 Intermittency in the transition to turbulence for a shear-thinning fluid in Hagen-Poiseuille flow. *J. Appl. Fluid Mech.* **7** (1), 1–6.
- BATCHELOR, G. K. & GILL, A. E. 1962 Analysis of the stability of axisymmetric jets. *J. Fluid Mech.* **14** (4), 529–551.
- BIRD, R. B., STEWART, W. E. & LIGHTFOOT, E. N. 2002 Transport phenomena. *Appl. Mech. Rev.* **55** (1), R1–R4.
- BOYD, J., BUICK, J. M. & GREEN, S. 2007 Analysis of the Casson and Carreau-Yasuda non-

- Newtonian blood models in steady and oscillatory flows using the lattice Boltzmann method. *Phys. Fluids* **19** (9), 093103.
- CARREAU, P. J. 1972 Rheological equations from molecular network theories. *Trans. Soc. Rheol.* **16** (1), 99–127.
- CARREAU, P. J., KEE, D. D. & DAROUX, M. 1979 An analysis of the viscous behaviour of polymeric solutions. *Can. J. Chem. Eng.* **57** (2), 135–140.
- CHARLES, A., PEIXINHO, J., RIBEIRO, T., AZIMI, S., ROCHER, V., BAUDEZ, J.-C. & BAHRANI, S. A. 2024 Asymmetry and intermittency in the rheo-inertial transition to turbulence in pipe flow. *Phys. Fluids* **36** (5), 054120.
- CHAUDHARY, I., GARG, P., SUBRAMANIAN, G. & SHANKAR, V. 2021 Linear instability of viscoelastic pipe flow. *J. Fluid Mech.* **908**, A11.
- COWLEY, S. J. & SMITH, F. T. 1985 On the stability of Poiseuille-Couette flow: a bifurcation from infinity. *J. Fluid Mech.* **156**, 83–100.
- DEGUCHI, K. & NAGATA, M. 2011 Bifurcations and instabilities in sliding Couette flow. *J. Fluid Mech.* **678**, 156–178.
- DEGUCHI, K. & WALTON, A. G. 2013 A swirling spiral wave solution in pipe flow. *J. Fluid Mech.* **737**, R2.
- DONG, M. & ZHANG, M. 2022 Asymptotic study of linear instability in a viscoelastic pipe flow. *J. Fluid Mech.* **935**, A28.
- ESCUDIER, M. P., NICKSON, A. K. & POOLE, R. J. 2009 Turbulent flow of viscoelastic shear-thinning liquids through a rectangular duct: quantification of turbulence anisotropy. *J. Non-Newton. Fluid Mech.* **160** (1), 2–10.
- ESCUDIER, M. P., POOLE, R. J., PRESTI, F., DALES, C., NOUAR, C., DESAUBRY, C., GRAHAM, L. & PULLUM, L. 2005 Observations of asymmetrical flow behaviour in transitional pipe flow of yield-stress and other shear-thinning liquids. *J. Non-Newton. Fluid Mech.* **127** (2–3), 143–155.
- ESMAEL, A. & NOUAR, C. 2008 Transitional flow of a yield-stress fluid in a pipe: evidence of a robust coherent structure. *Phys. Rev. E* **77** (5), 057302.
- FAISST, H. & ECKHARDT, B. 2003 Traveling waves in pipe flow. *Phys. Rev. Lett.* **91** (22), 224502.
- GARG, P., CHAUDHARY, I., KHALID, M., SHANKAR, V. & SUBRAMANIAN, G. 2018 Viscoelastic pipe flow is linearly unstable. *Phys. Rev. Lett.* **121** (2), 024502.
- GIJSEN, F. J. H., VAN DE VOSSE, F. N. & JANSSEN, J. D. 1999 The influence of the non-Newtonian properties of blood on the flow in large arteries: steady flow in a carotid bifurcation model. *J. Biomech.* **32** (6), 601–608.
- LIU, R. & LIU, Q. S. 2012 Nonmodal stability in Hagen-Poiseuille flow of a shear thinning fluid. *Phys. Rev. E* **85** (6), 066318.
- LÓPEZ-CARRANZA, S. N., JENNY, M. & NOUAR, C. 2012 Pipe flow of shear-thinning fluids. *C. R. Méc* **340** (8), 602–618.
- PICAUT, L., RONSIN, O., CAROLI, C. & BAUMBERGER, T. 2017 Experimental evidence of a helical, supercritical instability in pipe flow of shear thinning fluids. *Phys. Rev. Fluids* **2** (8), 083303.
- PLAUT, E., ROLAND, N. & NOUAR, C. 2017 Nonlinear waves with a threefold rotational symmetry in pipe flow: influence of a strongly shear-thinning rheology. *J. Fluid Mech.* **818**, 595–622.
- SCHMID, P. J. & HENNINGSON, D. S. 2001 *Stability and transition in shear flows*. New York, NY: Springer.
- WEDIN, H. & KERSWELL, R. R. 2004 Exact coherent structures in pipe flow: travelling wave solutions. *J. Fluid Mech.* **508**, 333–371.
- WEN, C., POOLE, R. J., WILLIS, A. P. & DENNIS, D. J. C. 2017 Experimental evidence of symmetry-breaking supercritical transition in pipe flow of shear-thinning fluids. *Phys. Rev. Fluids* **2** (3), 031901.
- WYGNANSKI, I. J. & CHAMPAGNE, F. H. 1973 On transition in a pipe. Part 1. The origin of puffs and slugs and the flow in a turbulent slug. *J. Fluid Mech.* **59** (2), 281–335.
- YASUDA, K. Y., ARMSTRONG, R. C. & COHEN, R. E. 1981 Shear flow properties of concentrated solutions of linear and star branched polystyrenes. *Rheol. Acta* **20** (2), 163–178.